

1 Basement topography and sediment thickness beneath 2 Antarctica's Ross Ice Shelf

3 M.D. Tankersley^{1,2}, H.J. Horgan¹, C.S. Siddoway³, F. Caratori Tontini^{2,4}, K.J.
4 Tinto⁵

5 ¹Antarctic Research Centre, Victoria University of Wellington, Wellington, New Zealand

6 ²GNS Science, Lower Hutt, New Zealand

7 ³Colorado College, Colorado Springs, CO, USA

8 ⁴University of Genova, Genova, Italy

9 ⁵Lamont-Doherty Earth Observatory, Columbia University, Palisades, NY, USA

10 Key Points:

- 11 • Aeromagnetic analysis reveals basement surface and evidence of fault-controlled
extensional basins beneath Antarctica's Ross Ice Shelf
- 12 • Active faults at Siple Coast likely influence ice streams through control of geother-
mal heat, groundwater, and glacioisostatic adjustments
- 13 • A basement high beneath Ross Ice Shelf spatially coincides with a lithospheric bound-
ary, with contrasting sedimentary basins on either side

17 **Abstract**

18 New geophysical data from Antarctica's Ross Embayment reveal the structure and
 19 subglacial geology of extended continental crust beneath the Ross Ice Shelf. We use air-
 20 borne magnetic data from the ROSETTA-Ice Project to locate the contact between mag-
 21 netic basement and overlying sediments. We delineate a broad, segmented basement high
 22 with thin (0-500m) non-magnetic sedimentary cover which trends northward into the Ross
 23 Sea's Central High. Before subsiding in the Oligocene, this feature likely facilitated early
 24 glaciation in the region and subsequently acted as a pinning point and ice flow divide.
 25 Flanking the high are wide sedimentary basins, up to 3700m deep, which parallel the Ross
 26 Sea basins and likely formed during Cretaceous-Neogene intracontinental extension. NW-
 27 SE basins beneath the Siple Coast grounding zone, by contrast, are narrow, deep, and
 28 elongate. They suggest tectonic divergence upon active faults that may localize geother-
 29 mal heat and/or groundwater flow, both important components of the subglacial sys-
 30 tem.

31 **Plain Language Summary**

32 The bedrock geology of Antarctica's southern Ross Embayment is concealed by 100s
 33 to 1000s of meters of sedimentary deposits, seawater, and the floating Ross Ice Shelf. Our
 34 research strips away those layers to discover the shape of the consolidated bedrock be-
 35 low, which we refer to as the basement. To do this, we use the contrast between non-
 36 magnetic sediments and magnetic basement rocks to map out the depth of the basement
 37 surface under the Ross Ice Shelf. Our primary data source is airborne measurements of
 38 the variation in Earth's magnetic field across the ice shelf, from flight lines spaced 10-
 39 km apart. We use the resulting basement topography to highlight sites of possible in-
 40 fluence upon the Antarctic Ice Sheet and to further understand the tectonic history of
 41 the region. We discover contrasting basement characteristics on either side of the ice shelf,
 42 separated by a N-S trending basement high. The West Antarctic side displays evidence
 43 of active faults, which may localize geothermal heat, accommodate movements of the solid
 44 earth caused by changes in the size of the Antarctic Ice Sheet, and control the flow of
 45 groundwater between the ice base and aquifers. This work addresses critical interactions
 46 between ice and the solid earth.

47 **1 Introduction**

48 The southern sector of Antarctica's Ross Embayment beneath the Ross Ice Shelf
 49 (RIS; area $\sim 480,000 \text{ km}^2$) is poorly resolved because the region is not accessible to con-
 50 ventional seismic or geophysical surveying. Rock exposures on land suggest that RIS crust
 51 consists of early Paleozoic post-orogenic sediments, intruded in places by mid-Paleozoic
 52 and Cretaceous granitoids (Luyendyk et al., 2003; Goodge, 2020). Following the onset
 53 of extension in the mid-Cretaceous, grabens formed and filled with terrestrial and ma-
 54 rine deposits, continuing into the Cenozoic (e.g. Sorlien et al., 2007; Coenen et al., 2019),
 55 as the Ross Embayment underwent thermal subsidence (Karner et al., 2005; Wilson &
 56 Luyendyk, 2009). The physiography of this region then responded to the onset of glacia-
 57 tion in the Oligocene (Paxman et al., 2019), coinciding with localized extension in the
 58 western Ross Sea until 11 Ma (Granot & Dyment, 2018). The Oligocene-early-Miocene
 59 paleo-landscape of the Ross Sea sector was revealed by marine seismic data (e.g. Bran-
 60 colini et al., 1995; Pérez et al., 2021) and offshore drilling that penetrated crystalline base-
 61 ment (DSDP Site 270; Ford & Barrett, 1975) (Figure 1). Recognition of the role of el-
 62 evated topography in Oligocene formation of the Antarctic Ice Sheet (DeConto & Pol-
 63 lard, 2003; Wilson et al., 2013) and the likely influence of subglacial topography upon
 64 ice sheet processes during some climate states (Austermann et al., 2015; Colleoni et al.,
 65 2018) motivated our effort to determine basement topography beneath the Ross Ice Shelf.

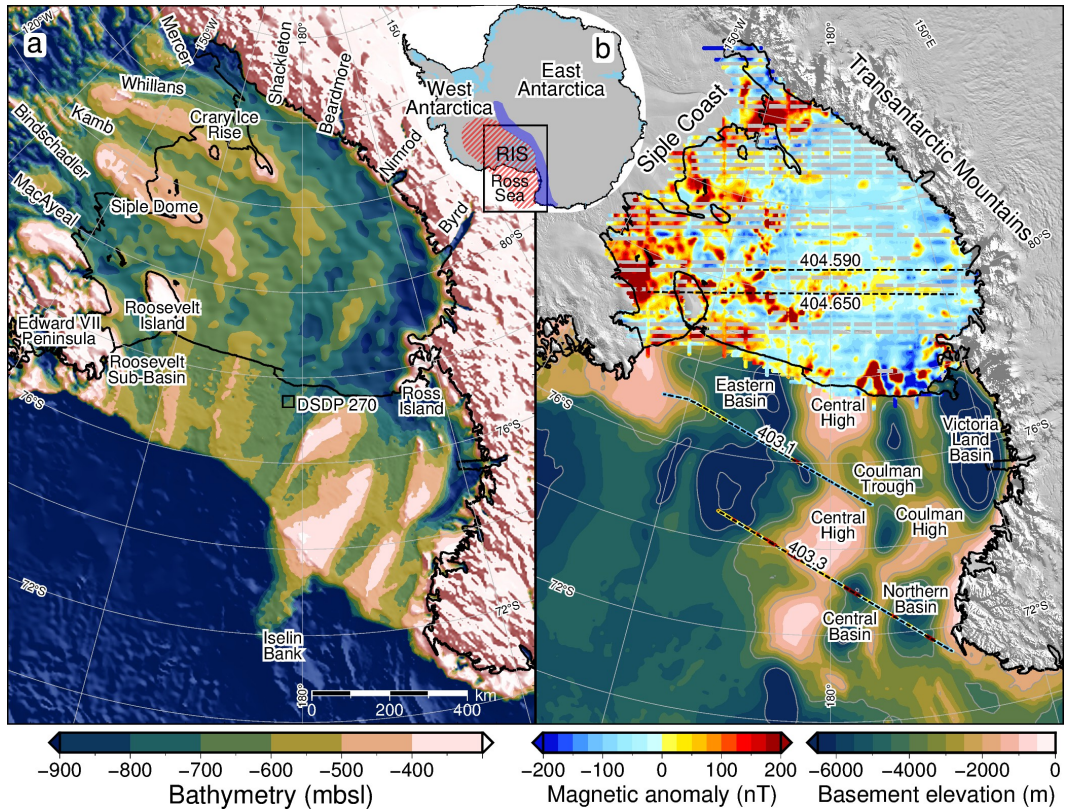


Figure 1. (a) Bathymetry and sub-ice bed elevations (Morlighem et al., 2020) including ROSETTA-Ice gravity-derived bathymetry (Tinto et al., 2019) beneath the Ross Ice Shelf (RIS). Labels include ice streams and outlet glaciers. (b) Basement elevation from ANTOSTRAT marine seismic compilation in the Ross Sea (Brancolini et al., 1995) and airborne magnetic data from ROSETTA-Ice (over RIS) and Operation IceBridge (black dashed lines). Inset map shows figure location, West Antarctic Rift System (hatched red), Transantarctic Mountains (dark blue), and ice shelves (light blue). Shelf edge, grounding line, and coastlines in black (Rignot et al., 2013). MODIS imagery from Scambos et al. (2007).

66 Ice sheet dynamics are of high interest in the RIS region because its grounding zone
 67 (GZ) and pinning points (Still et al., 2019) buttress Antarctica's second-largest drainage
 68 basin (Tinto et al., 2019). Our work in this sensitive region seeks to delimit the extent
 69 and geometry of competent basement because the margins of basement highs are sites
 70 of strong contrasts in permeability that influence the circulation of subglacial waters. A
 71 spectacular example of the confinement of subglacial water between the ice sheet and
 72 basement exists in ice radar profiles for the continental interior (Bell et al., 2011), but
 73 little is known about the subglacial hydrology of deep groundwater reservoirs within sediment-
 74 filled marine basins that receive terrestrial freshwater influx (Siegert et al., 2018; Gustafson
 75 et al., 2021). These basins may contain up to 50% of total subglacial freshwater (Christoffersen
 76 et al., 2014), where the discharge and recharge along fault-damage zones (Jolie et al., 2021)
 77 is controlled by pressure from the overriding ice sheet (Gooch et al., 2016). Possible ev-
 78 idence that RIS basement margins localize basinal waters, causing the advection of geother-
 79 mal heat, comes from elevated values and significant spatial variability of measured geother-
 80 mal heat flux (GHF) at points around the Ross Embayment (Begeman et al., 2017). Here
 81 we present the first map of magnetic basement topography and thickness of overlying
 82 non-magnetic sediments for the southern Ross Embayment, developed using ROSETTA-
 83 Ice (2015-2019) airborne magnetic data (Figure 1b, Tinto et al., 2019). Our work reveals
 84 three major sedimentary basins and a broad basement ridge that separates crust of con-
 85 trasting basement characteristics.

86 2 Data and Methods

87 We use ROSETTA-Ice aeromagnetic data to image the shallowest magnetic signals
 88 in the crust. Assuming that the overlying sediments and sedimentary rocks produce smaller
 89 magnetic anomalies than the crystalline basement, we treat the resulting solutions as the
 90 depth to the magnetic basement (Text S1). To do this, we implemented Werner decon-
 91 volution (Werner, 1953) on 2D moving and expanding windows of line data, isolating anom-
 92 alies and solving for their source parameters (Text S2, location, depth, susceptibility, body
 93 type). The resulting solutions are non-unique; each observed magnetic anomaly can be
 94 solved by bodies at multiple locations and depths by varying the source's magnetic sus-
 95 ceptibility and width. The result is a depth scatter of solutions (Figures 2 & S2), which
 96 tend to vertically cluster beneath the true source. This magnetic basement approach has
 97 been used to map sedimentary basins throughout Antarctica (i.e. Karner et al., 2005;
 98 Bell et al., 2006; Studinger et al., 2004; Frederick et al., 2016) where typically, the tops
 99 of solution clusters are manually selected to represent the basement depth. Our approach
 100 expands on this method by utilizing a reliable, automated method of draping a surface
 101 over these depth-scattered solutions to produce a continuous basement surface (Text S3-
 102 4).

103 We implemented a 2-step tuning process that ties our RIS magnetic basement to
 104 well-constrained seismic basement in the Ross Sea, from the Antarctic Offshore Stratig-
 105 raphy project (ANTOSTRAT) (Figure 1b, Brancolini et al., 1995). This involved using
 106 Operation IceBridge (OIB) airborne magnetic data (Cochran et al., 2014) collected over
 107 the RIS and Ross Sea. Minimizing misfits between OIB magnetic basement and ANTOSTRAT
 108 basement, as well as between OIB and ROSETTA-Ice magnetic basements, enabled tun-
 109 ing of our method to optimal basement depths (Figures 2, S2, S3e&f, Text S3-4).

110 Our RIS results (Figure S4) were merged with offshore ANTOSTRAT data (Brancolini
 111 et al., 1995) and smoothed with an 80km Gaussian filter to match the characteristic wave-
 112 lengths of the Ross Sea basement (Text S5). The combined grid (Figure 3a) was then
 113 subtracted from BedMachine bathymetry (Figure 1a, Text S6, Morlighem et al., 2020),
 114 to obtain the sediment thickness distribution for the Ross Embayment (Figure 3b).

115 These sub-RIS results together with free-air gravity data allowed us to infer the
 116 locations of regional scale faults beneath the RIS. Criteria used to locate faults include

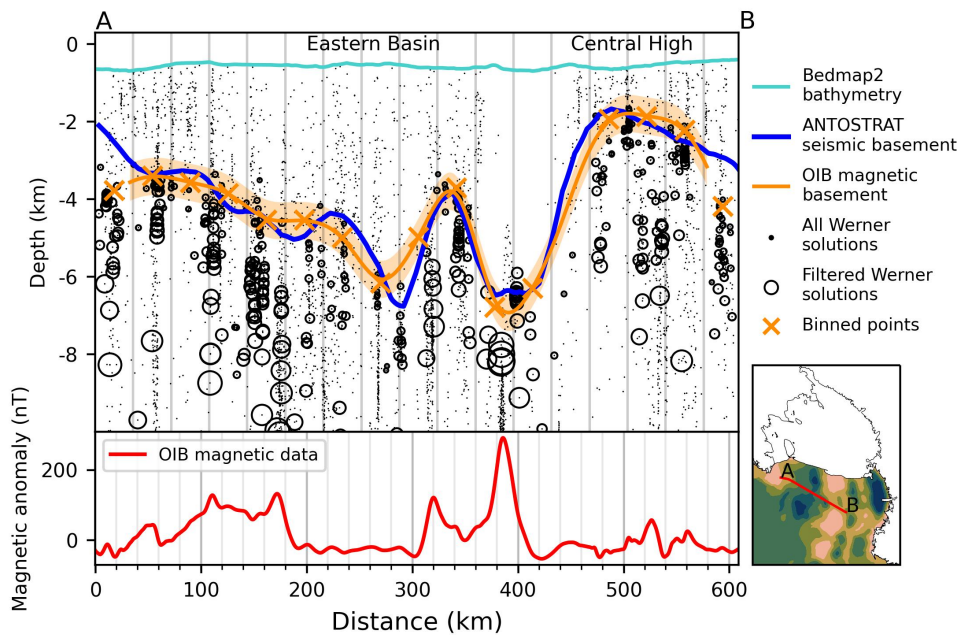


Figure 2. Ross Sea magnetic and seismic basement comparison. Operation IceBridge airborne magnetic data (lower panel) from segment 403.1 used in Werner deconvolution to produce magnetic anomaly source solutions (black dots). Filtering removed shallow solutions, and remaining solutions (circles scaled to magnetic susceptibility) were binned and interpolated to produce the magnetic basement (orange line with uncertainty band).

117 1) high relief on the magnetic basement surface, 2) linear trends that cross zones of shal-
 118 low basement, 3) high gradient gravity anomalies (Figure S1a, ROSETTA-Ice) and 4)
 119 large contrasts in sediment thickness. Narrow, deep, linear basins are likely to be con-
 120 trolled by active faults (e.g. Finn, 2002; Drenth et al., 2019). We display the inferred
 121 faults upon a base map of crustal stretching factors (β -factor; the ratio of crustal thick-
 122 ness before and after extension, Figure 4a), using an initial crustal thickness of 38km (Müller
 123 et al., 2007), a continent-wide Moho model (An et al., 2015), and our basement surface
 124 as the top of the crust (Text S6).

125 3 Results

126 We find that an almost continuous drape of sediment covers the RIS region (Fig-
 127 ure 3b), with only \sim 3% of the area having $<$ 200m of sedimentary cover. Prominent be-
 128 neath the midline of the RIS is a broad NNW-SSE trending basement ridge (Figure 3a,
 129 Mid-Shelf High; MSH), which comprises most of the shallowest ($<$ 700 meters below sea
 130 level (mbsl)) sub-RIS basement, with several regions with as little as 100m of sedimen-
 131 tary cover. Basement is deeper on the East Antarctic side of the MSH, where it aver-
 132 ages \sim 2400 mbsl, compared to an average depth of \sim 1900 mbsl on the West Antarctic
 133 side (Figure 3a histogram). Sedimentary fill is \sim 400m greater and more uniformly dis-
 134 tributed on the East Antarctic side than the West Antarctic side (Figure 3b histogram).

135 To estimate our uncertainty (Text S7), we examined the misfit between OIB and
 136 ANTOSTRAT basement (Figures 2 & S2) and between our basement and OIB basement
 137 (Figures S3e&f). There is a median misfit of 480m (22% of average RIS depth) for base-
 138 ment (Figure S5, Figure S6). A similar 470m median basement misfit is estimated by
 139 comparing our results to eight active source seismic surveys (Figure 3b, Table S1). In-
 140 corporating the \sim 70m uncertainty in the bathymetry model (Tinto et al., 2019), our rep-
 141 resentative sediment thickness uncertainty is 550m (37% of average RIS thickness, Fig-
 142 ure S5).

143 A single broad and deep basin (300 x 600km) separates the MSH and the Transantar-
 144 tic Mountains (TAM) (Figure 3a, Western Ross Basin). The Western Ross Basin par-
 145 allels the TAM and has the deepest-observed sub-RIS basement depths of 4500 mbsl, ac-
 146 ccommodating sediments up to 3800m thick (Figure 3b). It contains a long, narrow NW-
 147 SE trending ridge with \sim 1500m structural relief above the basement sub-basins on ei-
 148 ther side. Bordering the MSH on the east, an elongate NW-SE trending basin runs from
 149 the RIS calving front to the Siple Coast GZ (Figure 3a), where beneath Siple Dome we
 150 discover a 100x200km depocenter reaching basement depths up to 4000 mbsl, with sed-
 151 iments up to 3700m thick. We refer to this depocenter as Siple Dome Basin, a feature
 152 bounded on the east by a basement high that trends southward from Roosevelt Island.
 153 This high rises to its shallowest point at the GZ, where its sedimentary cover is less than
 154 100m. A second deep, narrow basin (50x200km in dimension) is found along the north
 155 margin of Crary Ice Rise, separated from the Siple Dome Basin by a NW-SE ridge un-
 156 derlying Kamb Ice Stream. The basin, labeled Crary Trough in Figure 3a, reaches base-
 157 ment depths of 3200 mbsl, with sediments 1800-2700m thick. The southernmost RIS has
 158 an additional depocenter with up to 2000m of fill beneath Whillans Ice Stream (loca-
 159 tion in Figure 1a).

160 Inferred active sub-RIS faults (Figures 4a & S1) correspond to narrow, linear base-
 161 ment basins with high-gradient gravity anomalies, prevalent on the West Antarctic side
 162 (Figure S1a). Inactive normal and strike-slip faults are inferred along lineaments that
 163 segment the shallow MSH into blocks and are oriented parallel to TAM outlet glacier
 164 faults. β -factors are indicative of thinned crust and are different on either side of the MSH.
 165 The TAM side shows higher β -factors (average 1.99) with low variability. The West Antarc-
 166 tic side has lower β -factors overall (average 1.82), but with some higher values up to 2.1
 167 (Figure 4a).

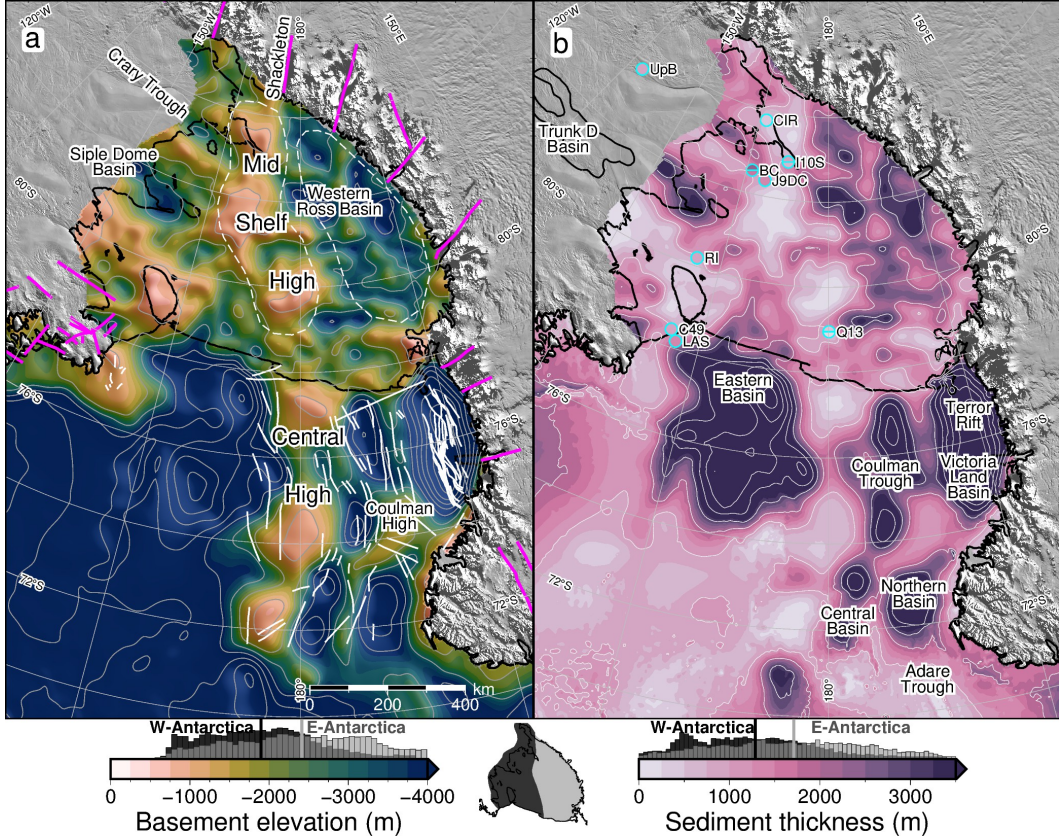


Figure 3. (a) Basement elevation (magnetic for Ross Ice Shelf (RIS), seismic elsewhere) contoured at 1km intervals. Pink lines are onshore mapped and inferred faults (Goodge, 2020; Siddoway, 2008; Ferraccioli et al., 2002). White lines are offshore faults (Salvini et al., 1997; Luyendyk et al., 2001; Chiappini et al., 2002; Sauli et al., 2021). Dashed white lines show Mid Shelf High and Western Ross Basin extents. (b) Sediment thickness contoured at 1km intervals. Previous basement-imaging RIS seismic surveys (Table S1) are plotted on same color scale, with upper and lower uncertainty ranges as circle halves, where reported. Trunk D Basin outlined in West Antarctica (Bell et al., 2006). Color scales for both a) and b) are set to sub-RIS data range. Colorbar histograms show data distribution for East vs West Antarctic sides of the sub-RIS, separated by the Mid-Shelf High. Inset map shows East vs West divide. Vertical lines on histograms denote average values of each side.

168 **4 Discussion**

169 Sub-RIS sedimentary basins align with and show lateral continuity with the Ross
 170 Sea's Roosevelt Sub-Basin, Eastern Basin, Coulman Trough, and Victoria Land Basin
 171 (Figure 3, e.g. Cooper et al., 1995). The MSH passes northward into the Ross Sea's promi-
 172 nent Central High (CH). At the southern RIS margin, the narrow Siple Dome Basin has
 173 continuity with the previously identified Trunk D Basin (Figure 3a, Bell et al., 2006).
 174 The throughgoing trends imply regional continuity of crustal structure and a common
 175 tectonic development of the Ross Sea and RIS regions. Our sediment thicknesses are com-
 176 patible with those determined by a) eight active-source seismic surveys (Figure 3b), for
 177 which the median misfit is 470m (Table S1), and b) surface wave dispersion indicating
 178 2-4km of sediment under the RIS, similar to our range, with the maximum beneath Crary
 179 Ice Rise (Zhou et al., 2022). Three additional western RIS seismic profiles report up to
 180 several kilometers of sediment, in general accordance with our results (Stern et al., 1991;
 181 ten Brink et al., 1993; Beaudoin et al., 1992). Additionally, machine learning applied to
 182 geophysical datasets predicts a high likelihood of sedimentary basins at the locations of
 183 Siple Dome Basin and Crary Trough (L. Li et al., 2021).

184 **4.1 West Antarctic Rift System extensional basins**

185 The Western Ross Basin has a configuration similar to the western Ross Sea rift
 186 basins (e.g. Salvini et al., 1997) with a broad and deep basin, separated into distinct de-
 187 pocenters by a linear, low relief ridge. The deeper of the depocenters, on the TAM side
 188 of the ridge, coincides with alternating high and low free-air gravity anomalies (Figure
 189 S1a). These similarities suggest the sub-RIS continuations of Coulman Trough and Vic-
 190 toria Land Basin (Figure 3b) likely share a common tectonic origin as fault-controlled
 191 basins (Figures 3a & 4a) formed through Cretaceous distributed continental extension
 192 across the WARS (Jordan et al., 2020). These sub-RIS basins terminate against the south-
 193 ern segment of the MSH (Figure 3a).

194 The linear ridge within the Western Ross Basin (Figure 3a) may be an expression
 195 of normal or oblique faults linked to the southward-narrowing Terror Rift (Sauli et al.,
 196 2021), formed due to Cenozoic oceanic spreading in the Adare Trough (Figure 3b, Gra-
 197 not & Dyment, 2018). The Western Ross Basin, with up to 3800m of fill, terminates along
 198 the prominent edge of the MSH that lines up with the fault-controlled trough and crustal
 199 boundary that passes southward beneath Shackleton Glacier (Borg et al., 1990). We in-
 200 terpret the basement lineament (Figure 4a) as a transfer fault separating sectors of crust
 201 extended to different degrees.

202 The southeastern RIS margin is distinguished by linear ridges and narrow, deep
 203 basins. The prominent NW-SE basement trends coincide with high-gradient gravity anom-
 204 alies (Figure S1a, Tinto et al., 2019) and thick sediments, suggesting normal fault con-
 205 trol and active divergent tectonics beneath the GZ. Our Siple Coast cross-section (Fig-
 206 ure 4b) displays dramatic basement relief, exceeding 2km, in the Siple Dome Basin and
 207 Crary Trough, which we attribute to displacement upon high angle faults. Portions of
 208 basin-bounding faults were previously detected by ground-based gravity surveys upon
 209 the Whillans Ice Stream flank (Figure 4a, Muto et al., 2013) and site J9DC (Figure 3b),
 210 where large variations in sediment thickness indicate up to 600m of fault throw (Greischar
 211 et al., 1992). The continuity between the narrow Siple Dome Basin (this study) and the
 212 Trunk D Basin (Figure 3a, Bell et al., 2006) suggests that the active tectonic domain con-
 213 tinues southward past the GZ. The fault-controlled tectonic basins may reflect a crustal
 214 response to the lithospheric foundering hypothesized beneath the South Pole region (Shen,
 215 Wiens, Stern, et al., 2018) or be a broader regional expression of Neogene extension that
 216 formed the Bentley Subglacial Trench (Lloyd et al., 2015).

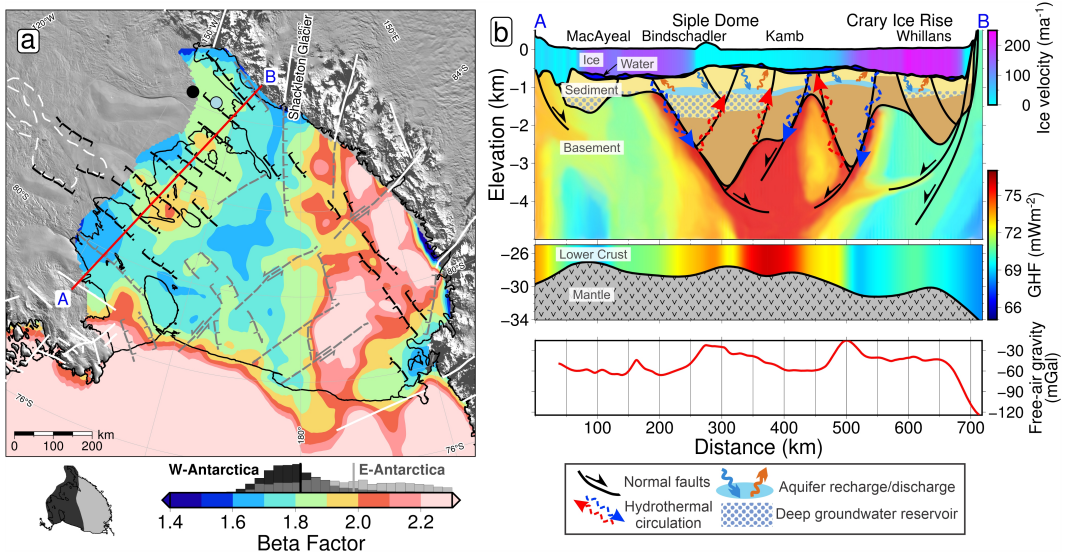


Figure 4. Tectonic interpretation of the sub-Ross Ice Shelf (RIS). **(a)** β stretching factors (Text S6). Colorbar histogram shows data distribution of West vs. East Antarctic sides, same as Figure 3. Black and grey lines indicate inferred active and inactive faults, respectively, with kinematics shown with half-arrows (strike or oblique-slip) and hachures (normal-sense). White lines show previously reported faults, same as Figure 3a. Dashed-white outline is Trunk D Basin (Bell et al., 2006). Black and blue dots show Subglacial Lake Whillans and sedimentary basin from Gustafson et al. (2021), respectively. Cross-section A-B in red. **(b)** Siple Coast cross-section from A-B, showing basin sediments bounded by faults, with geothermal heat flux (GHF) through the crust (lower panel from Burton-Johnson et al. (2020), upper panel interpreted). Ice surface, ice base, and bathymetry from Morlighem et al. (2020). Ice streams colored by velocity (Mouginot et al., 2019; Venturelli et al., 2020). Moho is from Shen, Wiens, Anandakrishnan, et al. (2018). Lower panel shows ROSETTA-Ice gravity. Named features are labeled on top.

217 **4.2 Consequences for ice sheet dynamics**

218 Our basement topography and suggested crustal faults likely exert a strong influence
 219 on the overriding ice, especially along the Siple Coast. Here, we show deep and thick
 220 sedimentary basins which likely contain voluminous basinal aquifers (Figure 4b; cf. Gustafson
 221 et al., 2021). Where these aquifers discharge along fault-damage zones, they can enhance
 222 GHF and promote basal melting (Gooch et al., 2016), as depicted in Figure 4a. The el-
 223 evated GHF seen at Subglacial Lake Whillans (285 mW/m^2 , Fisher et al., 2015) may
 224 arise from fault localization (Figure 4a). Confinement of the aquifers between the ice bed
 225 and low-permeability basement may promote fluid overpressure, enabling ice streaming
 226 (e.g. Ravier & Buoncristiani, 2018). Additionally, the Siple Coast faults likely accom-
 227 modate the solid Earth's response to fluctuating ice volume. A matter receiving consid-
 228 erable debate (Neuhaus et al., 2021; Venturelli et al., 2020; Lowry et al., 2019), is Kingslake
 229 et al.'s (2018) finding of rapid re-advance of the Siple Coast grounding zone following
 230 Holocene deglaciation. The re-advance was in part due to swift glacioisostatic rebound
 231 (cf. Lowry et al., 2020; Coulon et al., 2021), a process aided by the region's low-viscosity
 232 mantle (Whitehouse et al., 2019) and likely to be accommodated upon pre-existing crustal
 233 faults, as observed in the Lambert Graben (Phillips & Läufer, 2009). Our proposed graben-
 234 bounding faults would provide a tectonic control on the glacioisostatic adjustment of the
 235 Siple Coast region.

236 **4.3 Mid-Shelf High - Central High**

237 The 650-km-long Mid-Shelf High features three shallow, blocky segments $>150 \text{ km}$
 238 in breadth, which have only thin sediment cover ($<200\text{m}$). At their shallowest points,
 239 the top of basement lies within $\sim 300\text{m}$ of the ice shelf base, at a depth comparable to
 240 the basement high at Roosevelt Island. Roosevelt Island is a modern pinning point (Still
 241 et al., 2019) owing to the thicker sediment, there (Figure 3b). We introduce the MSH
 242 as a prominent pinning point at times of advance and greater extent of the Antarctic Ice
 243 Sheet, in keeping with evidence from subglacial sediment records that indicate a major
 244 ice flow divide between East and West Antarctic ice during and since Last Glacial Max-
 245 imum (X. Li et al., 2020; Licht et al., 2014; Coenen et al., 2019).

246 The prominence of the MSH is due in part to the contrasting geologic properties
 247 of the East versus West Antarctic type crust and their respective responses to WARS
 248 extension. We distinguished β -factors on the TAM-side that are high and uniform, in-
 249 dicating distributed crustal extension. The West Antarctic side displays lower β -factors
 250 overall, but with localized extreme thinning beneath Siple Coast (Figure 4a). The greater
 251 amount of extension on the East Antarctic side coincides with the deeper bathymetry
 252 (Figure 1a), deeper basement, and thicker sediments (Figure 3). The contrasting prop-
 253 erties are also evident in ROSETTA-Ice magnetic and gravity anomalies, used by Tinto
 254 et al. (2019) to identify a north-south trending tectonic boundary along the midline of
 255 Ross Embayment. The MSH in the magnetic basement coincides with and spans this bound-
 256 ary, which has been further substantiated by passive-seismic studies that show a lithospheric-
 257 scale boundary (Cheng et al., 2021; White-Gaynor et al., 2019). To the north, the fea-
 258 tures continue into the Ross Sea's Central High. Southward, the MSH basement feature
 259 trends into the TAM, where its western edge aligns with Shackleton Glacier, occupying
 260 a major fault separating the distinct geologic domains of the central and southern TAM
 261 (Borg et al., 1990; Paulsen et al., 2004), which also parallels a prominent magnetic lin-
 262 eament at the South Pole (Studinger et al., 2006). The structure may be an expression
 263 of the East Antarctic craton margin or a major intracontinental transform (Figure 4a,
 264 Studinger et al., 2006).

265 At the time of Oligocene initiation of the Antarctic Ice sheet, paleotopographic re-
 266 constructions of the proto-Ross Embayment depict a long, broad range, emergent above
 267 sea level (Paxman et al., 2019; Wilson et al., 2012), that we equate to the MSH-CH that

268 divides the Embayment. The CH hosted small ice caps with alpine glaciers formed during
 269 the initial glacial stage in the region (De Santis et al., 1995), and continental ice ex-
 270 panded to the outer Ross Sea continental shelf from those centers (Bart & De Santis,
 271 2012). Between the late Oligocene and mid-Miocene, the CH subsided by up to 500m
 272 (Leckie, 1983; Kulhanek et al., 2019), receiving 100's of meters of sediment cover (\sim 400m
 273 at DSDP 270; De Santis et al., 1995). The geophysical similarities and continuity between
 274 the Ross Sea's CH and the RIS's MSH imply a similar glaciation and subsidence history
 275 for the MSH. A terrestrial/alpine stage for the MSH helps to explain the region's poten-
 276 tial to hold the late Oligocene's larger-than-modern ice volumes (Wilson et al., 2013; Pekar
 277 et al., 2006), with the MSH-CH having a central role in Oligocene ice sheet development
 278 and the subsequent evolution of the ice sheet and ice shelf, as is documented in the Ross
 279 Sea (Halberstadt et al., 2016).

280 4.4 Thermal subsidence and sedimentation

281 Incorporating the updated basement basin extents and geometries into post-rift ther-
 282 mal subsidence modeling will enable better constrained paleotopographic reconstructions.
 283 For the sub-RIS, these reconstructions (Wilson et al., 2012; Paxman et al., 2019) use a
 284 post-Eocene subsidence model based on gravity-derived basin geometries and uniform
 285 β -factors (Wilson & Luyendyk, 2009). This model predicts uniform stretching of the east-
 286 ern sub-RIS from the ice front to the Siple Coast, while our β -factors show increasing
 287 stretching from the ice front to the Siple Coast. This observed additional thinning likely
 288 has resulted in more subsidence for Siple Dome and the north flank of Crary Ice Rise,
 289 which can now be accounted for in reconstructions. Our sediment thickness comparison
 290 with past models (Text S6, Wilson & Luyendyk, 2009) shows the majority of the sub-
 291 RIS, especially the Siple Coast, contains more total sediment than previously estimated
 292 (Figure S1f). Depending on the age of this sediment, reconstructions may need to ac-
 293 count for the additional sediment deposition and loading.

294 5 Conclusions

295 Here we present a depth to magnetic basement map for the Ross Ice Shelf (RIS)
 296 from Werner deconvolution of airborne magnetic data. The RIS magnetic basement is
 297 tied to Ross Sea seismic basement, providing the first synthetic view of Ross Embayment
 298 crustal structure. Using a bathymetry model, we obtain the sediment thickness distri-
 299 bution and calculate crustal extension factors for the sub-RIS. The extensional features
 300 we image, resulting from West Antarctic Rift System extension, have continuity with Ross
 301 Sea basement structures to the north, and the prominent Mid-Shelf High trends north-
 302 ward into the Ross Sea's Central High. This combined high separates East and West Antarc-
 303 tic type crust, affected by different degrees of continental extension. The Mid-Shelf High
 304 was likely subaerial in the Oligocene, able to support alpine ice caps in early Antarctic
 305 glaciation. Subsequently it formed a prominent pinning point and ice flow divide between
 306 the East and West Antarctic Ice Sheets.

307 Newly identified narrow, linear, deep sedimentary basins provide evidence of ac-
 308 tive faults beneath the Siple Coast grounding zone, where thinned crust overlying anomalous
 309 mantle (Shen, Wiens, Anandakrishnan, et al., 2018) likely experiences elevated geother-
 310 mal heat flow promoting the formation of subglacial water. Faults that control basement
 311 margins may accommodate motion caused by the glacioisostatic response to ice sheet
 312 volume changes. Subglacial sedimentary basins in this setting likely contain confined aquifers
 313 within permeable basin fill. Here, ice overburden pressure would control flow both be-
 314 tween and within the subglacial and groundwater systems, possibly localizing geother-
 315 mal heat. Updated sediment thickness and basin extents should be incorporated into new
 316 paleotopographic reconstructions of time intervals of interest for paleo-ice sheet mod-
 317 eling. Our work contributes critical information about Ross Embayment basement to-

318 topography and subglacial boundary conditions that arise from an interplay of geology, tec-
 319 tonics, and glaciation.

320 6 Open Research

321 ROSETTA-Ice and OIB magnetics data are available through <https://www.usapdc.org/view/project/p0010035>. Results from this study are available to download from
 322 <https://doi.pangaea.de/10.1594/PANGAEA.941238> and a Jupyter notebook documenting
 323 our workflow and figure creation is available at <https://zenodo.org/badge/latestdoi/470814953>.

325 Acknowledgments

326 Funding support from the New Zealand Ministry of Business and Innovation and Em-
 327 ployment through the Antarctic Science Platform contract (ANTA1801) Antarctic Ice
 328 Dynamics Project (ASP-021-01) and the National Science Foundation (1443497 and 1443534).
 329 We are grateful to Robin Bell, Isabel Cordero, Alec Lockett, Joel Wilner, Zoe Krauss,
 330 and the entire ROSETTA-Ice team for undertaking the ambitious data acquisition and
 331 processing effort. We thank Katharina Hochmuth and Guy Paxman for thoughtful re-
 332 views which greatly improved the manuscript, as well as Chris Sorlien, Tim Stern, Si-
 333 mon Lamb, Lara Pérez, Ryan Venturelli, Wei Ji Leong, and Dan Lowry for valuable in-
 334 put. Figures used GMT6/PyGMT (Wessel et al., 2019; Uieda et al., 2021), with a script
 335 adapted from Venturelli et al. (2020). Geosoft Oasis Montaj™ was used for magnetics
 336 processing and Werner deconvolution.

337 References

- 338 An, M., Wiens, D. A., Zhao, Y., Feng, M., Nyblade, A. A., Kanao, M., ... Lévêque,
 339 J.-J. (2015). S-velocity model and inferred Moho topography beneath
 340 the Antarctic Plate from Rayleigh waves: Antarctic S-velocities and Moho.
 341 *Journal of Geophysical Research: Solid Earth*, 120(1), 359–383. doi:
 342 10.1002/2014JB011332
- 343 Andrews, J. T., & LeMasurier, W. (2021). Resolving the argument about volcanic
 344 bedrock under the West Antarctic Ice Sheet and implications for ice sheet sta-
 345 bility and sea level change. *Earth and Planetary Science Letters*, 568, 117035.
 346 doi: 10.1016/j.epsl.2021.117035
- 347 Austermann, J., Pollard, D., Mitrovica, J. X., Moucha, R., Forte, A. M., DeConto,
 348 R. M., ... Raymo, M. E. (2015). The impact of dynamic topography change
 349 on Antarctic ice sheet stability during the mid-Pliocene warm period. *Geology*,
 350 43(10), 927–930. doi: 10.1130/G36988.1
- 351 Bart, P., & De Santis, L. (2012). Glacial intensification during the Neogene: A
 352 review of seismic stratigraphic evidence from the Ross Sea, Antarctica, conti-
 353 nental shelf. *Oceanography*, 25(3), 166–183. doi: 10.5670/oceanog.2012.92
- 354 Beaudoin, B. C., ten Brink, U. S., & Stern, T. A. (1992). Characteristics and pro-
 355 cessing of seismic data collected on thick, floating ice: Results from the Ross
 356 Ice Shelf, Antarctica. *Geophysics*, 57(10), 1359–1372. doi: 10.1190/1.1443205
- 357 Begeman, C. B., Tulaczyk, S. M., & Fisher, A. T. (2017). Spatially Variable
 358 Geothermal Heat Flux in West Antarctica: Evidence and Implications. *Geo-
 359 physical Research Letters*, 44(19), 9823–9832. doi: 10.1002/2017GL075579
- 360 Bell, R. E., Ferraccioli, F., Creyts, T. T., Braaten, D., Corr, H., Das, I., ...
 361 Wolovick, M. (2011). Widespread Persistent Thickening of the East Antarctic
 362 Ice Sheet by Freezing from the Base. *Science*, 331(6024), 1592–1595. doi:
 363 10.1126/science.1200109
- 364 Bell, R. E., Studinger, M., Karner, G., Finn, C. A., & Blankenship, D. D. (2006).
 365 Identifying major sedimentary basins beneath the West Antarctic Ice Sheet
 366 from aeromagnetic data analysis. In D. K. Fütterer, D. Damaske, G. Klein-

- 367 schmidt, H. Miller, & F. Tessensohn (Eds.), *Antarctica* (pp. 117–121).
 368 Berlin/Heidelberg: Springer-Verlag. doi: 10.1007/3-540-32934-X_13
- 369 Borg, S. G., Depaolo, D. J., & Smith, B. M. (1990). Isotopic structure and tectonics
 370 of the central Transantarctic mountains. *Journal of Geophysical Research*,
 371 95(B5), 6647. doi: 10.1029/JB095iB05p06647
- 372 Brancolini, G., Busetti, M., Marchetti, A., Santis, L. D., Zanolla, C., Cooper, A. K.,
 373 ... Hinze, K. (1995). Descriptive text for the seismic stratigraphic atlas of
 374 the Ross Sea, Antarctica. In A. K. Cooper, P. F. Barker, & G. Brancolini
 375 (Eds.), *Geology and Seismic Stratigraphy of the Antarctic Margin* (Vol. 68,
 376 p. A271-A286). Washington, D. C.: American Geophysical Union. doi:
 377 10.1002/9781118669013.app1
- 378 Burton-Johnson, A., Dziadek, R., & Martin, C. (2020). Geothermal heat flow in
 379 Antarctica: Current and future directions. *The Cryosphere Discussions*, 1–45.
 380 doi: 10.5194/tc-2020-59
- 381 Cheng, W., Hu, X. G., & Liu, L. T. (2021). Anisotropy Gradients in the Middle of
 382 the Ross Sea Embayment, West Antarctica: Evidence From QL Scattered Sur-
 383 face Waves. *Geophysical Research Letters*, 48(6). doi: 10.1029/2020GL091232
- 384 Chiappini, M., Ferraccioli, F., Bozzo, E., & Damaske, D. (2002). Regional compi-
 385 lation and analysis of aeromagnetic anomalies for the Transantarctic Moun-
 386 tains–Ross Sea sector of the Antarctic. *Tectonophysics*, 347(1-3), 121–137. doi:
 387 10.1016/S0040-1951(01)00241-4
- 388 Christoffersen, P., Bougamont, M., Carter, S. P., Fricker, H. A., & Tulaczyk, S.
 389 (2014). Significant groundwater contribution to Antarctic ice streams hy-
 390 drologic budget. *Geophysical Research Letters*, 41(6), 2003–2010. doi:
 391 10.1002/2014GL059250
- 392 Cochran, J. R., Burton, B., Frearson, N., & Tinto, K. (2014). IceBridge Scintrex
 393 CS-3 Cesium magnetometer L1B geolocated magnetic anomalies, version 2.
 394 [Line 403, 404]. Boulder, Colorado USA. NASA National Snow and Ice Data
 395 Center Distributed Active Archive Center. doi: 10.5067/OY7C2Y61YSYW
- 396 Coenen, J. J., Scherer, R. P., Baudooin, P., Warny, S., Castañeda, I. S., & Askin,
 397 R. (2019). Paleogene marine and terrestrial development of the West
 398 Antarctic Rift System. *Geophysical Research Letters*, 47(3). doi: 10.1029/
 399 2019GL085281
- 400 Colleoni, F., De Santis, L., Montoli, E., Olivo, E., Sorlien, C. C., Bart, P. J., ...
 401 Prato, S. (2018). Past continental shelf evolution increased Antarctic ice
 402 sheet sensitivity to climatic conditions. *Scientific Reports*, 8(1), 11323. doi:
 403 10.1038/s41598-018-29718-7
- 404 Cooper, A. K., Barker, P. F., & Brancolini, G. (Eds.). (1995). *Geology and seismic*
 405 *stratigraphy of the Antarctic margin* (No. v. 68). Washington, D.C: AGU. doi:
 406 10.1029/AR068
- 407 Coulon, V., Bulthuis, K., Whitehouse, P. L., Sun, S., Haubner, K., Zipf, L., & Pat-
 408 tyn, F. (2021). Contrasting response of West and East Antarctic Ice Sheets to
 409 glacial isostatic adjustment. *Journal of Geophysical Research: Earth Surface*,
 410 126(7). doi: 10.1029/2020JF006003
- 411 Cox, S., Smith Lyttle, B., & 2019, S. G. A. G. (2019). SCAR GeoMAP dataset.
 412 *GNS Science*. doi: 10.21420/7SH7-6K05
- 413 Crary, A. P. (1961). Marine-sediment thickness in the eastern Ross Sea area, Antarc-
 414 tica. *Geological Society of America Bulletin*, 72(5), 787. doi: 10.1130/0016
 415 -7606(1961)72[787:MTITER]2.0.CO;2
- 416 DeConto, R. M., & Pollard, D. (2003). A coupled climate–ice sheet mod-
 417 eling approach to the Early Cenozoic history of the Antarctic ice sheet.
 418 *Palaeogeography, Palaeoclimatology, Palaeoecology*, 198(1-2), 39–52. doi:
 419 10.1016/S0031-0182(03)00393-6
- 420 De Santis, L., Anderson, J. B., Brancolini, G., & Zayatz, I. (1995). Seismic record
 421 of late Oligocene through Miocene glaciation on the central and eastern conti-

- 422 nental shelf of the Ross Sea. In A. K. Cooper, P. F. Barker, & G. Brancolini
 423 (Eds.), *Antarctic Research Series* (pp. 235–260). Washington, D. C.: American
 424 Geophysical Union. doi: 10.1029/AR068p0235
- 425 Drenth, B. J., Grauch, V., Turner, K. J., Rodriguez, B. D., Thompson, R. A., &
 426 Bauer, P. W. (2019). A shallow rift basin segmented in space and time: The
 427 southern San Luis Basin, Rio Grande rift, northern New Mexico, U.S.A. *Rocky
 428 Mountain Geology*, 54(2), 97–131. doi: 10.24872/rmgjournal.54.2.97
- 429 Ferraccioli, F., Bozzo, E., & Damaske, D. (2002). Aeromagnetic signatures over
 430 western Marie Byrd Land provide insight into magmatic arc basement, mafic
 431 magmatism and structure of the Eastern Ross Sea Rift flank. *Tectonophysics*,
 432 347, 139–165. doi: 10.1016/S0040-1951(01)00242-6
- 433 Finn, C. (2002). *Examples of the utility of magnetic anomaly data for geologic map-*
 434 *ping* (Open-File Report No. 02-400). Denver, Colorado: USGS.
- 435 Fisher, A. T., Mankoff, K. D., Tulaczyk, S. M., Tyler, S. W., Foley, N., & and
 436 the WISSARD Science Team. (2015). High geothermal heat flux measured below the West Antarctic Ice Sheet. *Science Advances*, 1, 1–9. doi:
 437 10.1126/sciadv.1500093
- 438 Ford, A., & Barrett, P. J. (1975). *Basement rocks of the south-central Ross Sea, site*
 439 *270, DSDP leg 28* (Tech. Rep.). College Station, TX, United States: Texas A
 440 & M University, Ocean Drilling Program. doi: 10.2973/dsdp.proc.28.130.1975
- 441 Frederick, B. C., Young, D. A., Blankenship, D. D., Richter, T. G., Kempf, S. D.,
 442 Ferraccioli, F., & Siegert, M. J. (2016). Distribution of subglacial sediments
 443 across the Wilkes Subglacial Basin, East Antarctica. *Journal of Geophysical
 444 Research: Earth Surface*, 121(4), 790–813. doi: 10.1002/2015JF003760
- 445 Fretwell, P., Pritchard, H. D., Vaughan, D. G., Bamber, J. L., Barrand, N. E.,
 446 Bell, R. E., ... Zirizzotti, A. (2013). Bedmap2: Improved ice bed, surface
 447 and thickness datasets for Antarctica. *The Cryosphere*, 7(1), 375–393. doi:
 448 10.5194/tc-7-375-2013
- 449 Gooch, B. T., Young, D. A., & Blankenship, D. D. (2016). Potential groundwater
 450 and heterogeneous heat source contributions to ice sheet dynamics in critical
 451 submarine basins of East Antarctica. *Geochemistry, Geophysics, Geosystems*,
 452 17(2), 395–409. doi: 10.1002/2015GC006117
- 453 Goodge, J. W. (2020). Geological and tectonic evolution of the Transantarctic
 454 Mountains, from ancient craton to recent enigma. *Gondwana Research*, 80,
 455 50–122. doi: 10.1016/j.gr.2019.11.001
- 456 Granot, R., & Dyment, J. (2018). Late Cenozoic unification of East and
 457 West Antarctica. *Nature Communications*, 9(1), 3189. doi: 10.1038/
 458 s41467-018-05270-w
- 459 Greischar, L. L., Bentley, C. R., & Whiting, L. R. (1992). An analysis of gravity
 460 measurements on the Ross Ice Shelf, Antarctica. In *Contributions to Antarc-*
 461 *tic Research III* (pp. 105–155). American Geophysical Union (AGU). doi: 10
 462 .1029/AR057p0105
- 463 Gustafson, C., Key, K., Siegfried, M., Winberry, J. P., Fricker, H. A., Venturelli, R.,
 464 & Michaud, A. B. (2021). A deep and dynamic groundwater system beneath
 465 an Antarctic ice stream. In *AGU Fall Meeting 2021*. AGU.
- 466 Halberstadt, A. R. W., Simkins, L. M., Greenwood, S. L., & Anderson, J. B.
 467 (2016). Past ice-sheet behaviour: Retreat scenarios and changing con-
 468 trols in the Ross Sea, Antarctica. *The Cryosphere*, 10(3), 1003–1020. doi:
 469 10.5194/tc-10-1003-2016
- 470 Jolie, E., Scott, S., Faulds, J., Chambeffort, I., Axelsson, G., Gutiérrez-Negrín, L. C.,
 471 ... Zemedkun, M. T. (2021). Geological controls on geothermal resources for
 472 power generation. *Nature Reviews Earth & Environment*, 2(5), 324–339. doi:
 473 10.1038/s43017-021-00154-y
- 474 Jordan, T. A., Riley, T. R., & Siddoway, C. S. (2020). The geological history and
 475 evolution of West Antarctica. *Nature Reviews Earth & Environment*, 1, 117–

133. doi: 10.1038/s43017-019-0013-6

Karner, G. D., Studinger, M., & Bell, R. E. (2005). Gravity anomalies of sedimentary basins and their mechanical implications: Application to the Ross Sea basins, West Antarctica. *Earth and Planetary Science Letters*, 235, 577–596. doi: 10.1016/j.epsl.2005.04.016

Kingslake, J., Scherer, R. P., Albrecht, T., Coenen, J., Powell, R. D., Reese, R., ... Whitehouse, P. L. (2018). Extensive retreat and re-advance of the West Antarctic Ice Sheet during the Holocene. *Nature*, 558(7710), 430–434. doi: 10.1038/s41586-018-0208-x

Kulhanek, D. K., Levy, R. H., Clowes, C. D., Prebble, J. G., Rodelli, D., Jovanovic, L., ... Naish, T. R. (2019). Revised chronostratigraphy of DSDP Site 270 and late Oligocene to early Miocene paleoecology of the Ross Sea sector of Antarctica. *Global and Planetary Change*, 178, 46–64. doi: 10.1016/j.gloplacha.2019.04.002

Leckie, F. M. (1983). Late Oligocene-early Miocene glacial record of the Ross Sea, Antarctica: Evidence from DSDP Site 270. *Geology*, 11, 578–582. doi: 10.1130/0091-7613(1983)11<578:LOMGRO>2.0.CO;2

Li, L., Aitken, A., Lindsay, M., & Kulessa, B. (2021). *Subglacial sedimentary basins focus key vulnerabilities of the Antarctic ice-sheet* (Preprint). In Review. doi: 10.21203/rs.3.rs-1117673/v1

Li, X., Zattin, M., & Olivetti, V. (2020). Apatite fission track signatures of the Ross Sea ice flows during the Last Glacial Maximum. *Geochemistry, Geophysics, Geosystems*, 21(10), 1–21. doi: 10.1029/2019GC008749

Licht, K. J., Hennessy, A. J., & Welke, B. M. (2014). The U-Pb detrital zircon signature of West Antarctic ice stream tills in the Ross embayment, with implications for Last Glacial Maximum ice flow reconstructions. *Antarctic Science*, 26(6), 687–697. doi: 10.1017/S0954102014000315

Lindeque, A., Gohl, K., Wobbe, F., & Uenzelmann-Neben, G. (2016). Preglacial to glacial sediment thickness grids for the Southern Pacific Margin of West Antarctica: Preglacial, transitional and full glacial isopach maps, West Antarctica. *Geochemistry, Geophysics, Geosystems*, 17(10), 4276–4285. doi: 10.1002/2016GC006401

Lloyd, A. J., Wiens, D. A., Nyblade, A. A., Anandakrishnan, S., Aster, R. C., Huerta, A. D., ... Zhao, D. (2015). A seismic transect across West Antarctica: Evidence for mantle thermal anomalies beneath the Bentley Subglacial Trench and the Marie Byrd Land Dome. *Journal of Geophysical Research: Solid Earth*, 120(12), 8439–8460. doi: 10.1002/2015JB012455

Lowry, D. P., Golledge, N. R., Bertler, N. A., Jones, R. S., McKay, R., & Stutz, J. (2020). Geologic controls on ice sheet sensitivity to deglacial climate forcing in the Ross Embayment, Antarctica. *Quaternary Science Advances*, 1, 1–17. doi: 10.1016/j.qsa.2020.100002

Lowry, D. P., Golledge, N. R., Bertler, N. A. N., Jones, R. S., & McKay, R. (2019, August). Deglacial grounding-line retreat in the Ross Embayment, Antarctica, controlled by ocean and atmosphere forcing. *Science Advances*, 5, 1–12. doi: 10.1126/sciadv.aav8754

Luyendyk, B., Sorlien, C. C., Wilson, D. S., Bartek, L. R., & Siddoway, C. S. (2001). Structural and tectonic evolution of the Ross Sea rift in the Cape Colbeck region, Eastern Ross Sea, Antarctica. *Tectonics*, 20(6), 933–958. doi: 10.1029/2000TC001260

Luyendyk, B., Wilson, D. S., & Siddoway, C. S. (2003). Eastern margin of the Ross Sea Rift in western Marie Byrd Land, Antarctica: Crustal structure and tectonic development. *Geochemistry, Geophysics, Geosystems*, 4(10), 1–25. doi: 10.1029/2002GC000462

Mooney, W. D., Laske, G., & Masters, T. G. (1998). CRUST 5.1: A global crustal model at $5^\circ \times 5^\circ$. *Journal of Geophysical Research: Solid Earth*, 103(B1), 727–

- 532 747. doi: 10.1029/97JB02122
- 533 Morlighem, M., Rignot, E., Binder, T., Blankenship, D., Drews, R., Eagles, G., ...
 534 Young, D. A. (2020). Deep glacial troughs and stabilizing ridges unveiled
 535 beneath the margins of the Antarctic ice sheet. *Nature Geoscience*, 13(2),
 536 132–137. doi: 10.1038/s41561-019-0510-8
- 537 Mouginot, J., Rignot, E., & Scheuchl, B. (2019). Continent-wide, interferometric
 538 SAR phase, mapping of Antarctic ice velocity. *Geophysical Research Letters*,
 539 46(16), 9710–9718. doi: 10.1029/2019GL083826
- 540 Müller, R. D., Gohl, K., Cande, S. C., Goncharov, A., & Golynsky, A. V. (2007).
 541 Eocene to Miocene geometry of the West Antarctic Rift System. *Aus-
 542 tralian Journal of Earth Sciences*, 54(8), 1033–1045. doi: 10.1080/
 543 08120090701615691
- 544 Muto, A., Christianson, K., Horgan, H. J., Anandakrishnan, S., & Alley, R. B.
 545 (2013). Bathymetry and geological structures beneath the Ross Ice Shelf at the
 546 mouth of Whillans Ice Stream, West Antarctica, modeled from ground-based
 547 gravity measurements. *Journal of Geophysical Research: Solid Earth*, 118(8),
 548 4535–4546. doi: 10.1002/jgrb.50315
- 549 Neuhaus, S. U., Tulaczyk, S. M., Stansell, N. D., Coenen, J. J., Scherer, R. P.,
 550 Mikucki, J. A., & Powell, R. D. (2021). Did Holocene climate changes
 551 drive West Antarctic grounding line retreat and readvance? *The Cryosphere*,
 552 15(10), 4655–4673. doi: 10.5194/tc-15-4655-2021
- 553 Paulsen, T., Encarnación, J., & Grunow, A. (2004). Structure and timing of
 554 transpressional deformation in the Shackleton Glacier area, Ross orogen,
 555 Antarctica. *Journal of the Geological Society*, 161(6), 1027–1038. doi:
 556 10.1144/0016-764903-040
- 557 Paxman, G. J. G., Jamieson, S. S., Hochmuth, K., Gohl, K., Bentley, M. J.,
 558 Leitchenkov, G., & Ferraccioli, F. (2019). Reconstructions of Antarctic to-
 559 topography since the Eocene–Oligocene boundary. *Palaeogeography, Palaeoclima-
 560 tology, Palaeoecology*, 535, 109346. doi: 10.1016/j.palaeo.2019.109346
- 561 Pekar, S. F., DeConto, R. M., & Harwood, D. M. (2006). Resolving a late
 562 Oligocene conundrum: Deep-sea warming and Antarctic glaciation. *Palaeo-
 563 geography, Palaeoclimatology, Palaeoecology*, 231, 29–40. doi: 10.1016/
 564 j.palaeo.2005.07.024
- 565 Pérez, L. F., De Santis, L., McKay, R. M., Larter, R. D., Ash, J., Bart, P. J., ...
 566 374 Scientists, I. O. D. P. E. (2021). Early and middle Miocene ice sheet
 567 dynamics in the Ross Sea: Results from integrated core-log-seismic interpreta-
 568 tion. *GSA Bulletin*. doi: 10.1130/B35814.1
- 569 Phillips, G., & Läufer, A. (2009). Brittle deformation relating to the Carbonif-
 570 erous–Cretaceous evolution of the Lambert Graben, East Antarctica: A pre-
 571 cursor for Cenozoic relief development in an intraplate and glaciated region.
 572 *Tectonophysics*, 471(3-4), 216–224. doi: 10.1016/j.tecto.2009.02.012
- 573 Ravier, E., & Buoncristiani, J.-F. (2018). Glaciohydrogeology. In *Past Glacial Envi-
 574 ronments* (pp. 431–466). Elsevier. doi: 10.1016/B978-0-08-100524-8.00013-0
- 575 Rignot, E., Jacobs, S., Mouginot, J., & Scheuchl, B. (2013). Ice-Shelf Melt-
 576 ing Around Antarctica. *Science*, 341(6143), 266–270. doi: 10.1126/
 577 science.1235798
- 578 Robertson, J. D., & Bentley, C. R. (1989). The Ross Ice Shelf: Glaciology and geo-
 579 physics paper 3: Seismic studies on the grid western half of the Ross Ice Shelf:
 580 RIGGS I and RIGGS II. In C. R. Bentley & D. E. Hayes (Eds.), *Antarctic Re-
 581 search Series* (Vol. 42, pp. 55–86). Washington, D. C.: American Geophysical
 582 Union. doi: 10.1029/AR042p0055
- 583 Rooney, S. T., Blankenship, D. D., & Bentley, C. R. (1987). Seismic refraction
 584 measurements of crustal structure in West Antarctica. In G. D. Mckenzie
 585 (Ed.), *Geophysical Monograph Series* (pp. 1–7). Washington, D. C.: American
 586 Geophysical Union. doi: 10.1029/GM040p0001

- 587 Salvini, F., Brancolini, G., Busetti, M., Storti, F., Mazzarini, F., & Coren, F. (1997).
 588 Cenozoic geodynamics of the Ross Sea region, Antarctica: Crustal extension,
 589 intraplate strike-slip faulting, and tectonic inheritance. *Journal of Geophysical
 590 Research: Solid Earth*, *102*(B11), 24669–24696. doi: 10.1029/97JB01643
- 591 Sauli, C., Sorlien, C., Busetti, M., De Santis, L., Geletti, R., Wardell, N., &
 592 Luyendyk, B. P. (2021). Neogene development of the Terror Rift, western
 593 Ross Sea, Antarctica. *Geochemistry, Geophysics, Geosystems*, *22*(3). doi:
 594 10.1029/2020GC009076
- 595 Scambos, T., Haran, T., Fahnestock, M., Painter, T., & Bohlander, J. (2007).
 596 MODIS-based Mosaic of Antarctica (MOA) data sets: Continent-wide surface
 597 morphology and snow grain size. *Remote Sensing of Environment*, *111*(2-3),
 598 242–257. doi: 10.1016/j.rse.2006.12.020
- 599 Shen, W., Wiens, D. A., Anandakrishnan, S., Aster, R. C., Gerstoft, P., Bromirski,
 600 P. D., ... Winberry, J. P. (2018). The crust and upper mantle structure of
 601 Central and West Antarctica from bayesian inversion of Rayleigh wave and
 602 receiver functions. *Journal of Geophysical Research: Solid Earth*, *123*(9),
 603 7824–7849. doi: 10.1029/2017JB015346
- 604 Shen, W., Wiens, D. A., Stern, T., Anandakrishnan, S., Aster, R. C., Dalziel, I., ...
 605 Winberry, J. P. (2018). Seismic evidence for lithospheric foundering beneath
 606 the southern Transantarctic Mountains, Antarctica. *Geology*, *46*(1), 71–74.
 607 doi: 10.1130/G39555.1
- 608 Siddoway, C. S. (2008). Tectonics of the West Antarctic Rift System: New
 609 light on the history and dynamics of distributed intracontinental exten-
 610 sion. In A. K. Cooper et al. (Eds.), *Antarctica: A Keystone in a Chang-
 611 ing World*. Washington DC: The National Academies Press. doi: 10.3133/
 612 ofr20071047KP09
- 613 Siegert, M. J., Kulessa, B., Bougamont, M., Christoffersen, P., Key, K., Andersen,
 614 K. R., ... Smith, A. M. (2018). Antarctic subglacial groundwater: A con-
 615 cept paper on its measurement and potential influence on ice flow. *Geological
 616 Society, London, Special Publications*, *461*(1), 197–213. doi: 10.1144/SP461.8
- 617 Smith, W. H. F., & Wessel, P. (1990). Gridding with continuous curvature splines in
 618 tension. *GEOPHYSICS*, *55*(3), 293–305. doi: 10.1190/1.1442837
- 619 Sorlien, C. C., Luyendyk, B., Wilson, D. S., Decesari, R. C., Bartek, L. R., &
 620 Diebold, J. B. (2007). Oligocene development of the West Antarctic
 621 Ice Sheet recorded in eastern Ross Sea strata. *Geology*, *35*(5), 467. doi:
 622 10.1130/G23387A.1
- 623 Stern, T. A., Davey, F. J., & Delisle, G. (1991). Lithospheric flexure induced by the
 624 load of the Ross Archipelago, southern Victoria land, Antarctica. In M. Thom-
 625 son, A. Crame, & J. Thomson (Eds.), *Geological Evolution of Antarctica* (pp.
 626 323–328). Cambridge, UK: Cambridge University Press.
- 627 Still, H., Campbell, A., & Hulbe, C. (2019). Mechanical analysis of pinning points
 628 in the Ross Ice Shelf, Antarctica. *Annals of Glaciology*, *60*(78), 32–41. doi: 10
 629 .1017/aog.2018.31
- 630 Studinger, M., Bell, R., Fitzgerald, P., & Buck, W. (2006). Crustal architecture of
 631 the Transantarctic Mountains between the Scott and Reedy Glacier region and
 632 South Pole from aerogeophysical data. *Earth and Planetary Science Letters*,
 633 *250*(1-2), 182–199. doi: 10.1016/j.epsl.2006.07.035
- 634 Studinger, M., Bell, R. E., Buck, W., Karner, G. D., & Blankenship, D. D. (2004).
 635 Sub-ice geology inland of the Transantarctic Mountains in light of new aero-
 636 geophysical data. *Earth and Planetary Science Letters*, *220*(3-4), 391–408. doi:
 637 10.1016/S0012-821X(04)00066-4
- 638 ten Brink, U. S., Bannister, S., Beaudoin, B. C., & Stern, T. A. (1993). Geophysical
 639 investigations of the tectonic boundary between East and West Antarctica.
 640 *Science*, *261*(5117), 45–50. doi: 10.1126/science.261.5117.45
- 641 Tinto, K. J., Padman, L., Siddoway, C. S., Springer, S. R., Fricker, H. A., Das, I.,

- 642 ... Bell, R. E. (2019). Ross Ice Shelf response to climate driven by the tec-
643 tonic imprint on seafloor bathymetry. *Nature Geoscience*, 12(6), 441–449. doi:
644 10.1038/s41561-019-0370-2
- 645 Uieda, L., Tian, D., Leong, W. J., Jones, M., Schlitzer, W., Toney, L., ... Quinn, J.
646 (2021). *PyGMT: A Python interface for the Generic Mapping Tools*. Zenodo.
647 doi: 10.5281/zenodo.5607255
- 648 Venturelli, R. A., Siegfried, M. R., Roush, K. A., Li, W., Burnett, J., Zook, R., ...
649 Rosenheim, B. E. (2020). Mid-Holocene grounding line retreat and read-
650 vance at Whillans Ice Stream, West Antarctica. *Geophysical Research Letters*,
651 47(15). doi: 10.1029/2020GL088476
- 652 Werner, S. (1953). Interpretation of magnetic anomalies at sheet-like bodies. In
653 *Sveriges Geologiska Undersok* (pp. 413–449). Stockholm Norstedt.
- 654 Wessel, P., Luis, J. F., Uieda, L., Scharroo, R., Wobbe, F., Smith, W. H. F., & Tian,
655 D. (2019). The Generic Mapping Tools version 6. *Geochemistry, Geophysics,
656 Geosystems*, 20(11), 5556–5564. doi: 10.1029/2019GC008515
- 657 White-Gaynor, A. L., Nyblade, A. A., Aster, R. C., Wiens, D. A., Bromirski, P. D.,
658 Gerstoft, P., ... Anandakrishnan, S. (2019). Heterogeneous upper man-
659 tle structure beneath the Ross Sea Embayment and Marie Byrd Land, West
660 Antarctica, revealed by P-wave tomography. *Earth and Planetary Science
661 Letters*, 513, 40–50. doi: 10.1016/j.epsl.2019.02.013
- 662 Whitehouse, P. L., Gomez, N., King, M. A., & Wiens, D. A. (2019). Solid Earth
663 change and the evolution of the Antarctic Ice Sheet. *Nature Communications*,
664 10(1), 503. doi: 10.1038/s41467-018-08068-y
- 665 Wilson, D. S., Jamieson, S. S., Barrett, P. J., Leitchenkov, G., Gohl, K., & Larter,
666 R. D. (2012). Antarctic topography at the Eocene–Oligocene boundary.
667 *Palaeogeography, Palaeoclimatology, Palaeoecology*, 335–336, 24–34. doi:
668 10.1016/j.palaeo.2011.05.028
- 669 Wilson, D. S., & Luyendyk, B. (2009). West Antarctic paleotopography estimated at
670 the Eocene–Oligocene climate transition. *Geophysical Research Letters*, 36(16),
671 L16302. doi: 10.1029/2009GL039297
- 672 Wilson, D. S., Pollard, D., DeConto, R. M., Jamieson, S. S., & Luyendyk, B. (2013).
673 Initiation of the West Antarctic Ice Sheet and estimates of total Antarctic
674 ice volume in the earliest Oligocene. *Geophysical Research Letters*, 40(16),
675 4305–4309. doi: 10.1002/grl.50797
- 676 Zhou, Z., Wiens, D. A., Shen, W., Aster, R. C., Nyblade, A., & Wilson, T. J.
677 (2022). Radial Anisotropy and Sediment Thickness of West and Central
678 Antarctica Estimated From Rayleigh and Love Wave Velocities. *Journal of
679 Geophysical Research: Solid Earth*, 127(3). doi: 10.1029/2021JB022857